

Design of Underwater Thruster Fault Detection Model Based on Vibration Sensor Data: Generative Adversarial Network-based Fault Data Expansion Approach for Data Imbalance

Myungjun Kim,¹ Hyunjoon Cho,^{2,3} Ki-Beom Choo,^{2,3} Huang Jiafeng,^{2,3}
Dong-Wook Jung,⁴ Jung-Hyeun Park,² Ji-Hyeong Lee,⁵
Sang-Ki Jeong,⁵ Dae-Hyeong Ji,⁶ and Hyeung-Sik Choi^{2*}

¹Maritime R&D Center, LIG Nex1 Co., Ltd, Gyeonggi-do 13488, Republic of Korea

²Department of Mechanical Engineering, Korea Maritime and Ocean University, Busan 49112, Republic of Korea

³Interdisciplinary Major of Ocean Renewable Energy Engineering, Korea Maritime and Ocean University, Busan 49112, Republic of Korea

⁴Underwater Vehicle Research Center, Korea Maritime and Ocean University, Busan 49112, Republic of Korea

⁵Maritime ICT R&D Center, Korea Institute of Ocean Science and Technology, Busan 49111, Republic of Korea

⁶Marine Security and Safety Research Center, Korea Institute of Ocean Science and Technology, Busan 49111, Republic of Korea

(Received June 15, 2022; accepted July 26, 2022)

Keywords: fault detection, underwater thruster, vibration data, confusion matrix, generative adversarial network, long short-term memory

The underwater thruster is an essential driving element for underwater platforms. Since underwater thrusters may fail because of external factors, a fault detection system is necessary for reliability and safety. Among the underwater thruster fault detection and diagnosis methods, a data-driven learning method, which does not require expertise or a physical model of the platform, is applied because a rule-based method lacks flexibility and a model-based method relies heavily on expertise. Although high-quality, large-capacity datasets are essential to implementing data-driven fault detection systems, the amount of fault sensor data is relatively scarce because most underwater thrusters operate in a normal state. However, if the platform is operated in a fault state for a long time to acquire fault sensor data, performance degradation of the thruster or accidents may result. In this study, we investigated a fault detection system wherein a small number of vibration sensor datasets were used as inputs for a generative adversarial network (GAN), and new vibration sensor datasets were generated, extended, and applied to a long short-term memory neural network for fault detection in an underwater thruster. For the defects detected by the machine learning algorithm, the rotor imbalance due to a thruster blade fault or the entanglement of floating objects was analyzed. To collect the vibration sensor dataset of the thruster, a structure for an underwater experiment was designed, and a system with a stable power supply, thruster control, and the capability to acquire vibration data was developed. Vibration sensor data obtained from the experiment and those generated by the GAN were comparatively analyzed in terms of their vibration characteristics using the fast Fourier transform. After training the neural network with GAN-generated data, the fault detection system was validated using real data as prediction data.

*Corresponding author: e-mail: hchoi@kmou.ac.kr
<https://doi.org/10.18494/SAM3991>

1. Introduction

Unmanned surface vehicles, autonomous underwater vehicles, and underwater manipulators operated in subsea environments use underwater thrusters or electric motors as actuators.^(1–4) Faults may occur in the thrusters owing to external factors, which may adversely affect the mission performance.⁽⁵⁾ To minimize the loss occurring in these thrusters, considerable research has been undertaken on fault detection and diagnosis systems related to motor-based underwater thrusters.⁽⁶⁾ The fault diagnostic methods can be categorized into rule-based, model-based, and data-driven approaches.⁽⁷⁾ The rule-based method operates by a sequential process of rules, and this method can be effectively used in a system that repeats a specific operation, as reported by Yang *et al.*⁽⁸⁾ However, in the event of unexpected faults, taking effective response measures is difficult; maintenance also becomes more difficult with the addition of new rules.^(8,9) Model-based methods have advantages over rule-based techniques, such as early detection of sudden or instantaneous small defects and increased process monitoring capabilities; however, they require knowledge of basic mathematical structures and dynamic process models.⁽⁹⁾

Data-driven methods can directly extract the features contained in data.⁽¹⁰⁾ Compared with model-based methods, the fault detection and diagnostic system for these methods can be constructed with a simpler model design, and data-driven methods are widely employed in a variety of fields.⁽¹⁰⁾ Among the data-driven methods, deep learning is an efficient data-based solution that allows the acquisition of data features.⁽¹¹⁾ For reliable learning performance with the data-training-based deep learning method, high-quality data in large volumes is a prerequisite.⁽¹²⁾ In recent data-driven fault detection and diagnosis studies, Ji *et al.* acquired data by implementing and operating the platform's thruster blade breakage for the fault diagnosis of an autonomous underwater vehicle on the basis of deep learning,⁽¹³⁾ and Chu *et al.* validated a fault detection system by referring to a vast dataset acquired in the past.⁽¹⁴⁾

However, if the platform is operated in a fault state for a long time to acquire data, performance degradation of the thruster, accidents, or platform loss may occur, or significant time and cost may be required to acquire a vast stored dataset from the past. In addition, most fault detection systems generally operate in a normal state owing to the low amount of fault data and large amount of normal data, which causes an imbalance problem.⁽¹⁵⁾ To prevent this, the present study generated new datasets by using pre-existing ones under normal and fault conditions, acquired for a short time as input data of a generative adversarial network (GAN). A long short-term memory (LSTM) neural network was trained with the normal and fault datasets generated by the GAN, and fault detection was performed for an underwater thruster. The data generation function of the GAN—an unsupervised learning task—was used to resolve the imbalance between fault data and normal data and reduce the platform operation time for data acquisition. The vibration features of the generated vibration data and those obtained through the experiments were compared and verified using the fast Fourier transform (FFT). The verified generated datasets were used to train the LSTM neural network used for time-series feature extraction. The LSTM neural network is a deep learning technique used to extract the features of time-series data. Zhang showed that it was more suitable than the convolutional neural network for railway track circuit fault detection and diagnosis.⁽¹⁶⁾ The LSTM model has been applied for various types of fault detection such as fault

detection in wind turbines⁽¹⁷⁾ and to assess the condition of bearings.⁽¹⁸⁾ In the present study, the LSTM neural network trained with the generated data was compared with one trained with real data. The sensor data used for detecting the faults of an underwater thruster may include voltage, rotational speed, current, and vibration. Among them, since vibration sensor data in a rotating machine generates characteristic data depending on the operating conditions of the rotating equipment, it is possible to identify faults in the rotating machine by analyzing the vibration data.⁽¹⁹⁾ Our study designed a fault detection system to obtain normal and fault vibration datasets of the underwater thruster. The fault detected through deep learning was rotor imbalance, which can occur because of blade damage of the thruster or the entanglement of floating objects.⁽²⁰⁾

2. Materials and Methods

2.1 GAN

GAN (Fig. 1) is a deep learning model that generates similar datasets from sample data through comparison between a generative model (G) and a discriminative model (D). Equation (1) shows the optimization equation of the GAN.⁽²¹⁾

$$\min_G \max_D V(G, D) = \mathbb{E}_{x \sim p_{data}(x)} [\log D(x)] + \mathbb{E}_{z \sim p_z(z)} [\log(1 - D(G(z)))] \quad (1)$$

Here, p_{data} refers to the real data distribution, and $p_z(z)$ is the prior distribution of input noise variable z from using the data distribution of generator p_g to train against x . $p_z(z)$ is mapped to $G(z; \theta_g)$ in the data space. $G(z; \theta_g)$ is the generated data and a parameter of G , and $D(x; \theta_d)$ represents the probability of receiving both real data and generated data as inputs and sorting through them to obtain the real data. Using $G(z; \theta_g)$, through iterative training, the resulting value of $\log(1 - D(G(z)))$ is outputted as $-\infty$, thus achieving the minimum value required to generate fake data, which is the same as that of the real data samples. Using parameter $D(x; \theta_d)$, through iterative training, $V(D, G) = 0$ is obtained as a result of calculating $\log D(x)$ and $\log(1 - D(G(z)))$; the maximum value is outputted and updated to discriminate between the real data and generated data. The network optimization equation of the GAN is based on the Nash equilibrium of the two-player game.

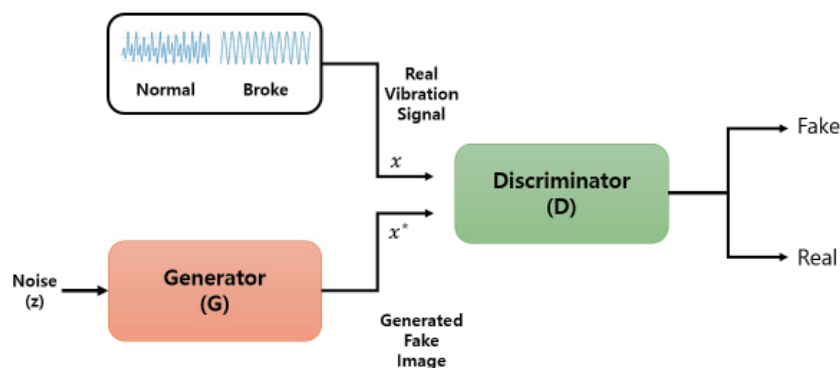


Fig. 1. (Color online) GAN diagram.

2.2 LSTM

In a recurrent neural network (RNN), the resulting value is outputted through the activation function at the node of the hidden layer and sent as the input for the subsequent calculation of the hidden layer, which allows the dynamic information to be modeled at various scales. However, when training with large-scale data, gradient disappearance or explosion occurs during the transition from the output layer to the input layer due to the limitation of “tanh” in the backpropagation process. LSTM resolves the problem of long-term dependences of the RNN by using the input, forget, and output gates. The role of gates is to discard or retain information of the input data that pass through the gate so that the data can be selectively adjusted. The gates use a sigmoid activation function, and a value between 0 and 1 is outputted depending on whether the input data can pass through the gate. The structure of the memory cell, which is the main component of the LSTM neural network, is shown in Fig. 2.⁽²²⁾

In Fig. 2, h_t and $x(t)$ are the output and input of the current step, respectively, and h_{t-1} is the hidden output state of the previous step. σ is the sigmoid function, and \tanh is the hyperbolic tangent function. C_t is a memory cell that stores information introduced from the previous step, and the output value from each gate is applied to C_t . There are three types of gates: forget gate, input gate, and output gate.

$$f(t) = \sigma(W_{xf}x(t) + W_{hf}h_{t-1} + b_f) \quad (2)$$

$$i(t) = \sigma(W_{ix}x(t) + W_{ih}h_{t-1} + b_i) \quad (3)$$

$$\tilde{C}(t) = \Phi(W_c \cdot [h_{t-1}, x_t] + b_c) \quad (4)$$

$$o(t) = \sigma(W_{ox}x(t) + W_{oh}h_{t-1} + b_o) \quad (5)$$

$$h(t) = \Phi(s(t)) * o(t) \quad (6)$$

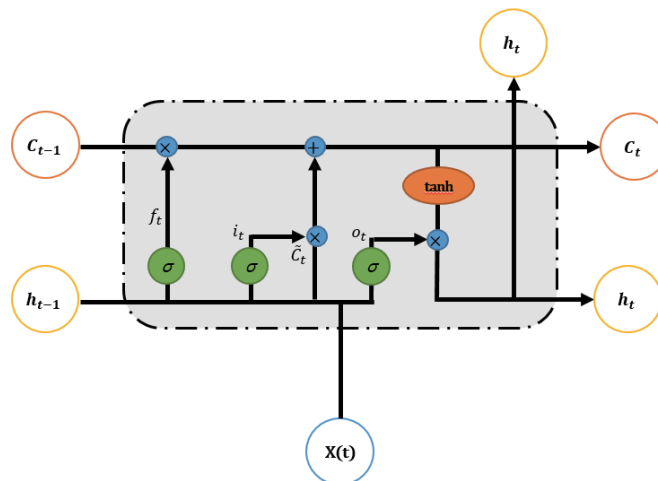


Fig. 2. (Color online) LSTM diagram.

$$C_t = f_t * C_{t-1} + i_t * \tilde{C}_t \quad (7)$$

In the above equations, W_{ix} , W_{fh} , and b_i represent the input weight matrix, hidden weight matrix, and bias vector, respectively. σ , Φ , and $*$ denote the sigmoid function, tanh function, and the product of two vectors by element, respectively. The forget gate decides which unnecessary information should be forgotten by considering the current input and previous output. The formula for calculating the forget gate is given by Eq. (2). The input gate determines how much information of the current input data is stored. The calculation formula for the input gate is given by Eq. (3). Equation (4) represents the tanh layer, which creates a vector of new candidate values to be added to the cell state. The output gate determines the extent to which the final cell state value is tuned. The formula for calculating the output gate is given by Eq. (5). Equation (6) is the formula of the cell state, and the output of each gate is updated in the cell state. The newly obtained cell state (C_t) is transferred to the next sequence.

2.3 Confusion matrix

The confusion matrix is used to evaluate the performance of the classification model. The rows of the matrix represent the actual labels of the classification types, and the columns represent the results predicted by the classification model. Therefore, the diagonal elements indicate correct classification results, and other values indicate incorrect classification results.⁽²³⁾ The confusion matrix is shown in Fig. 3.

Based on the confusion matrix, the following definitions for classification model performance measurement can be used.

$$Accuracy = \frac{TP + TN}{TP + FN + FP + TN} \quad (8)$$

$$Precision = \frac{TP}{TP + FP} \quad (9)$$

		Predicted	
		Actual	
Actual	TP(True Positive)	FP(False negative)	
	FP(False positive)	TN(True negative)	

Fig. 3. (Color online) Confusion matrix.

$$Recall = \frac{TP}{TP + FN} \quad (10)$$

$$F - score = \frac{2 \times Precision \times Recall}{Precision + Recall} \quad (11)$$

In Eqs. (8)–(11), accuracy is the fraction of all prediction results that match the actual label results, precision is the ratio of correct matching of the actual label among the results predicted by the model as positive, and recall is the ratio at which the model predicts that the actual label is defined as positive. F-score (F₁ score) is the harmonic average of precision and recall and is used to evaluate the performance of the classification model.⁽²⁴⁾

2.4 Composition of fault detection

The system proposed in this study was constructed to acquire sample data for the fault detection of underwater thrusters based on data training. As shown in Fig. 4, the system configuration includes the operator's computer, fault detection system, underwater thruster platform, and vibration sensor. The fault detection system controls the underwater thruster and simultaneously collects the vibration sensor data and transmits it to the operator's computer. The received vibration sensor data was saved to the created C# program.

The configuration of the fabricated fault detection system is shown in Fig. 5, where the main power supply, control board, and AC–DC converter are placed in the system.

PSoC 5LP micro controller units were used as the main controller. Three PSoC 5LPs were installed; the first PSoC communicated with the operator's computer to receive the thruster control signal and transmit the acquired vibration sensor data, the second controlled the thruster according to the thruster control signal, and the third received the vibration data from the vibration sensor. The underwater thruster was installed in an indoor water tank, as shown in Fig. 6. The vibration sensor was attached to the thruster body, and tests were performed at a depth of 5 m.

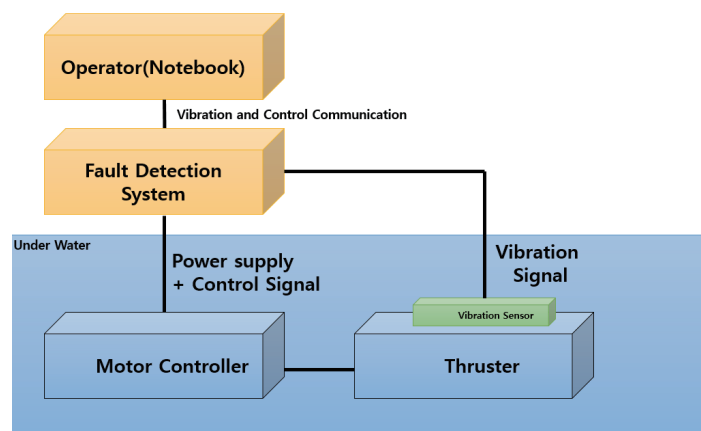


Fig. 4. (Color online) Fault detection platform.

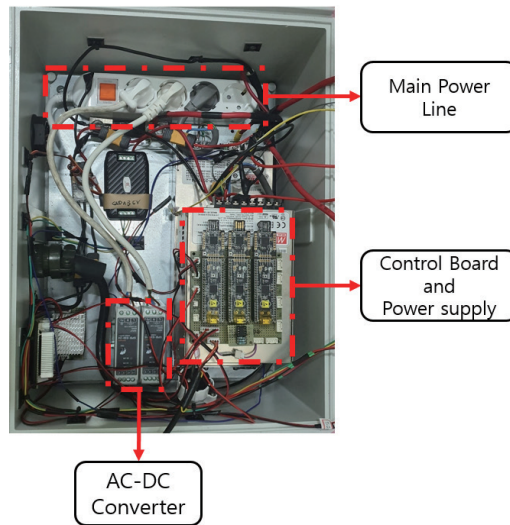


Fig. 5. (Color online) Fault detection system.

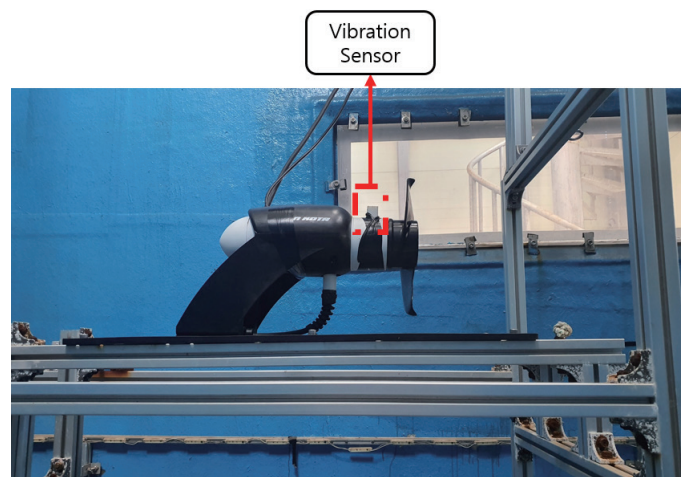


Fig. 6. (Color online) Underwater thruster.

2.5 Fault detection algorithm

According to Kemp *et al.*,⁽²⁵⁾ there are various types of faults related to underwater thrusters, such as software errors, entanglement, and loss of propeller blades. In this study, among the types of faults, those related to damage to the thruster blade due to external factors were selected for analysis. The vibration data were used as an indicator for diagnosing the thruster condition; moreover, the vibration data could characterize the features of the rotor imbalance fault, such as wing damage or floating object entanglement. Figure 7 shows an overview of the algorithm for fault detection.

A GAN is used to increase the amount of data acquired in a short time using a fault detection platform. Random noise is used as input data for the generator network to acquire the extended

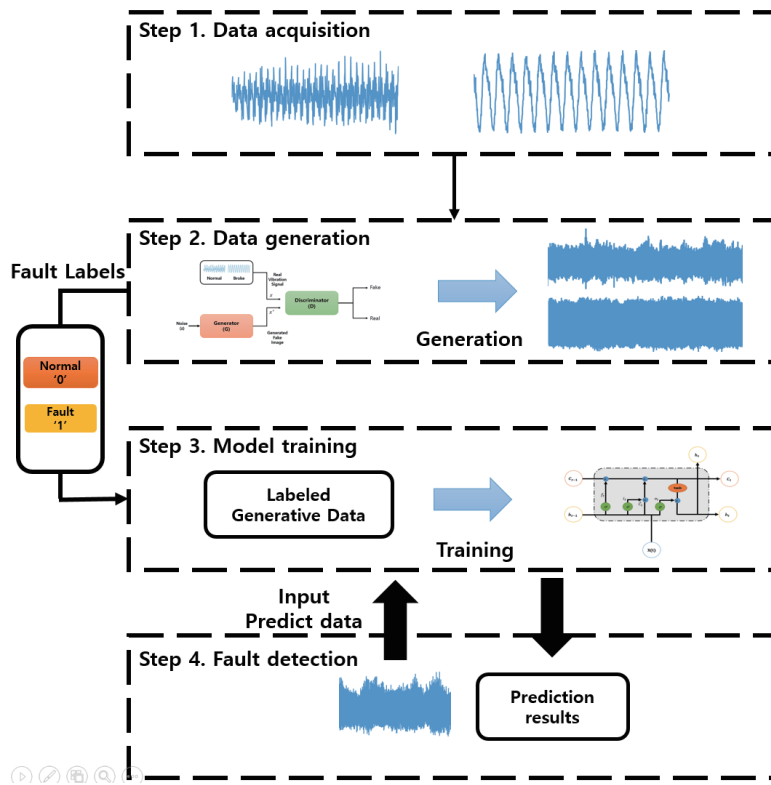


Fig. 7. (Color online) Fault detection algorithm.

datasets. After labeling the generated datasets as “normal” and “fault,” they are used for training with a classification LSTM neural network, with the loss function set to “Binary cross entropy”, which can perform binary classification. The resulting value of the neural network is outputted as any value of the sigmoid function between 0 and 1. Normal and fault data obtained through the experiments were used in the datasets for evaluation. This method not only increases the number of training datasets but also resolves the problem of data imbalance.

2.6 Data generation and LSTM network

After acquiring the normal and fault datasets using the fault detection system, extended sample datasets were generated using the GAN. Normal and fault data were extended using the method shown in Fig. 8.

In this study, a generation model was constructed using a simple dense layer activated by the tanh function for the generator. The discriminator was composed of convolutional layers, and the Rectified Linear Unit (ReLU) activation function was set for the entire network. The dropout rate was set to 25%, and the Adam optimization algorithm was used for optimization. The discrete Fourier transform (DFT) was used to compare and analyze the generated data and obtain the frequency and amplitude of the vibration data. The change in the center of mass due to the damage of the thruster had a proportional relationship with the rotation speed, and the amplitude of vibration was increased at the same frequency. The DFT is expressed as follows:

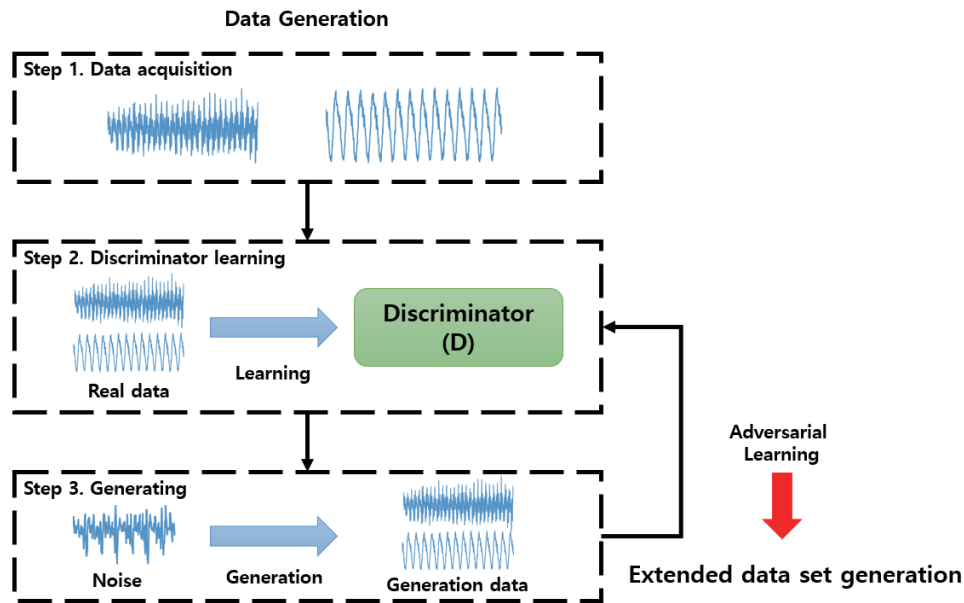


Fig. 8. (Color online) Extended dataset generation.

$$X(K) = \sum_{n=0}^{N-1} x(n)x(n)e^{-j\frac{2\pi kn}{N}}. \quad (12)$$

The validated extended datasets were used as training data for the LSTM neural network. According to the Nyquist–Shannon theorem, the complete f_{max} can be obtained by measurements at intervals of $1/2f_{max}$, assuming that the maximum frequency component of the analog signal to be measured is f_{max} . That is, at a specific sampling rate (f_s), the condition $f_s = 2f_{max}$ should be satisfied. In this study, approximately 20 Hz was sufficient to detect vibration data of approximately 9.2 Hz based on the Nyquist–Shannon theorem, but data at 100 Hz were used as training data to detect the features such as an accurate vibration distribution in addition to the shaft rotation frequency. The loss function used was “Binary cross entropy,” and the activation function was set to “sigmoid”.

3. Results and Discussion

3.1 Data acquisition experiment according to the underwater thruster condition

A data acquisition experiment based on the underwater thruster condition was conducted in a water tank. Images of the underwater experiment in the water tank are shown in Fig. 9.

For the vibration sensor data used in this study, the data of two conditions of the blade, which are a normal condition and a fault condition with the loss of blade thrust, were collected at a rotation speed of 550 rpm. The sampling frequency of the data for each condition was set to 100 Hz.



Fig. 9. (Color online) Underwater experiment.

3.2 Comparative validation of GAN generation data

For the GAN input data, we used 1000 data points each for normal and fault vibration sensor data, which were acquired by the data acquisition experiment using the underwater thruster. Using the GAN, vibration data (40000 points each) in the normal and fault conditions were generated. The generated data were comparatively analyzed using real data acquired through the experiment under the same conditions as those utilized for collecting the GAN input data. The DCT was performed with the vibration data, and the FFT was used. The results of the FFT analysis of 10000 data points are shown in Fig. 10.

According to the research by Betta *et al.*,⁽¹⁹⁾ vibration occurs at the shaft rotation frequency for a rotating machine under normal conditions, but when the defect of rotor imbalance occurs, high-intensity radial vibration occurs simultaneously. In the graph of Fig. 10(a), a vibration was found at 9.17 Hz using FFT of the real data under the normal condition, and vibration occurred at 9.2 Hz in the extended datasets generated through GAN. The value of 9.17 Hz can be converted to 550 rpm and be used as an estimate of the shaft rotation frequency component. From Fig. 10(b), as a result of the FFT of the real data under the damaged condition of the thruster, we found that the vibration magnitude was approximately four times higher than that of the normal condition at 9.47 Hz; the rotational speed also increased. The value of 9.47 Hz can be converted to 568 rpm, an increase of approximately 10 rpm from that of the normal condition. Table 1 outlines the results of the comparative verification between the real data and extended data using the FFT. When the vibration characteristics were analyzed on the basis of 20000 real data points, we found that the shaft rotation frequency was 9.47 Hz, the magnitude of the vibration was 23.27×10^{-2} g, and the vibration characteristics of the extended data were 9.43 Hz and 25.05×10^{-2} g, which were similar to those for the real data. In the case of more than 30000 vibration data points, the magnitude of the vibration tended to be dispersed around the shaft rotation frequency and decreased to 11.18×10^{-2} g; however, it can be seen that the vibration characteristics of the extended data were similar to those of the real data.

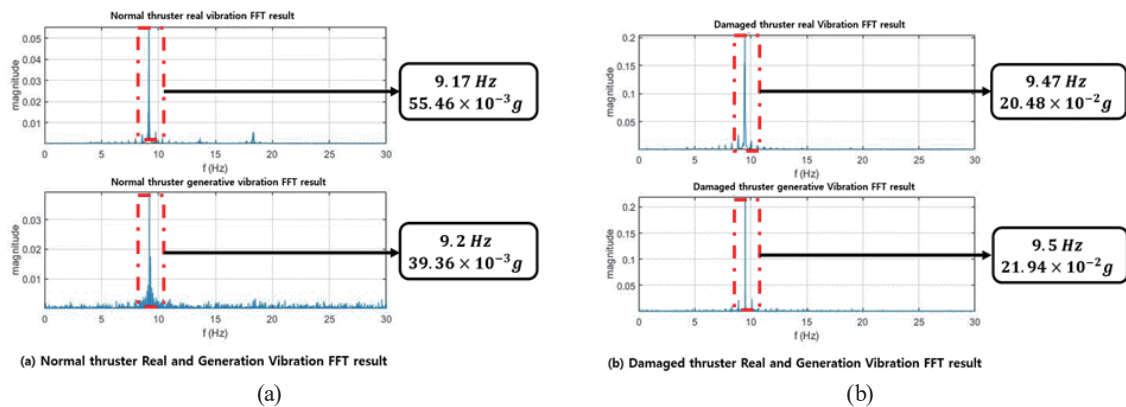


Fig. 10. (Color online) (a) Results of FFT for real and generation normal data and (b) results of FFT for real and generation damaged data.

Table 1
Results of FFT of real and generated data.

Number of data (EA)	Real data (Hz and g)		Generation data (Hz and g)	
10000	9.47	20.48×10^{-2}	9.5	21.94×10^{-2}
20000	9.38	23.27×10^{-2}	9.43	25.05×10^{-2}
30000	9.39	11.18×10^{-2}	9.35	10.68×10^{-2}
40000	9.38	13.00×10^{-2}	9.35	12.84×10^{-2}

3.3 Results of fault detection using LSTM

For the training data, the normal and fault data that were generated and extended were divided into groups of 100, making a total of 800 datasets. For data labeling, “0” indicated normal and “1” indicated damaged. The training sets and test sets were divided in a ratio of 7.5:2.5. The experimental datasets measured at different hours were used as the prediction data to perform fault detection. A total of 5000 experimental data points were used as LSTM prediction data, and the results of the prediction are shown in Fig. 11.

The plot in Fig. 11(a) shows the cases wherein, when the real data of the normal condition were predicted by the LSTM neural network, the normal condition was predicted. The plot in Fig. 11(b) shows the cases wherein, when the real data of the fault condition were predicted by the LSTM neural network, the fault condition was derived as the prediction result. The confusion matrix for the performance evaluation of the LSTM-based fault detection model is shown in Fig. 12.

According to the confusion matrix for the performance evaluation of the classification model with a test set consisting of 100 normal datasets and 100 fault datasets, all of the normal datasets were predicted to be normal. In the fault dataset, 97 were predicted to be faulty, and 3 were predicted to be normal. The precision, recall, and F-score results obtained from the confusion matrix are shown in Table 2.

The results demonstrated that when fault data (for which there is fewer data available than for normal data) are used as input data for the GAN to obtain extended datasets, the extended datasets can be utilized as training data for deep-learning-based fault detection/diagnosis systems such as LSTM.

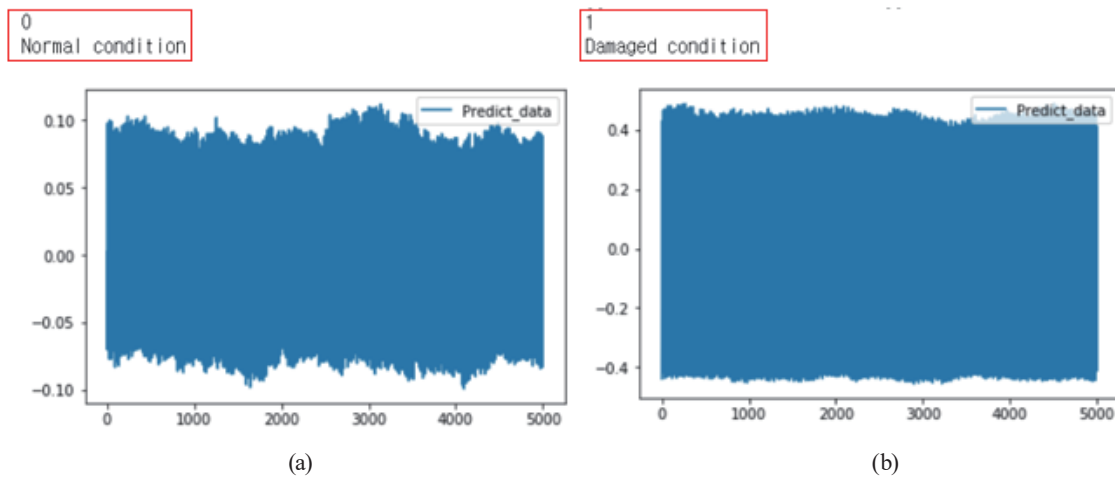


Fig. 11. (Color online) (a) LSTM prediction result of normal and (b) LSTM prediction result of fault.

		Predicted	
		Normal	Fault
Actual	Normal	100	0
	Fault	3	97

Fig. 12. (Color online) Confusion matrix of performance evaluation.

Table 2
Classification model performance evaluation results.

Precision (%)	100
Recall (%)	97
F-score (%)	98.48

4. Conclusion

In this study, we used a small number of vibration sensor datasets of an underwater thruster, measured in a short time, as inputs for a GAN to generate and extend new vibration datasets. We also investigated a fault detection system for an underwater thruster using an LSTM neural network. To collect the vibration sensor datasets of the thruster, we designed a structure for an underwater experiment, and we constructed a fault detection system with a stable power supply, thruster

control, and the capability to acquire vibration data. For the vibration sensor data acquired through the underwater experiment and those generated and extended by the GAN, their vibration characteristics were compared and validated using the FFT. As a result, the vibration characteristics of the generated and extended data were similar to those of real data. To verify that the extended datasets could be used as training data, an LSTM neural network was constructed. After training it with extended datasets, excellent performance was confirmed for predicting the condition of the underwater thruster. These results indicate that the fault data of underwater thrusters measured in a short time can be extended to a GAN and used for data-based fault detection systems.

Acknowledgments

This work was supported by the Unmanned Vehicles Core Technology Research and Development Program through the National Research Foundation of Korea (NRF) and Unmanned Vehicle Advanced Research Center (UVARC), funded by the Ministry of Science and ICT, the Republic of Korea (NRF-2020M3C1C1A02086321) and was a part of the Development of Unmanned Remotely Construction Aided System for Harbor Infrastructure Project, funded by the Ministry of Oceans and Fisheries, Korea.

References

- 1 E. Ormedic and G. Roberts: Control Eng. Pract. 12 (2004) 1575. <https://doi.org/10.1016/j.conengprac.2003.12.014>
- 2 J. Chae, T. Yeu, Y. Lee, Y. Lee, and S.-M. Yoon: J. Ocean Eng. Technol. 34 (2020) 180.
- 3 D. S. Nam, D. G. Lee, J. D. Ryu, and K. N. Ha: Proc. Eng. Technol. Innov. 12 (2019) 21.
- 4 D. W. Jung, S. M. Hong, J. H. Lee, H. J. Cho, H. S. Choi, and M. T. Vu: Proc. Engin. Technol. Innov. 9 (2018) 17
- 5 E. Omerdic, G. N. Roberts, and P. Ridao: IFAC Proc. 36 (2003) 127. [https://doi.org/10.1016/S1474-6670\(17\)37795-9](https://doi.org/10.1016/S1474-6670(17)37795-9)
- 6 S. M. Zanoli, G. Astolfi, G. Bruzzone, M. Bibuli, and M. Caccia: IFAC Proc. 45 (2012) 287. <https://doi.org/10.3182/20120919-3-IT-2046.00049>
- 7 B. Y. Raanan, J. Bellingham, Y. Zhang, M. Kemp, B. Kieft, H. Singh, and Y. Girdhar: J. Field Robot. 35 (2017) 705. <https://doi.org/10.1002/rob.21771>
- 8 H. Yang, S. Cho, C. S. Tae, and M. Zaheeruddin: Energy Convers. Manag. 49 (2008) 2291. <https://doi.org/10.1016/j.enconman.2008.01.029>
- 9 Z. Gao, C. Cetati, and S. X. Ding: IEEE Trans. Ind. Electron. 62 (2015) 3757. <https://doi.org/10.1109/TIE.2015.2417501>
- 10 S. Yin, S. X. Ding, X. Xie, and H. Luo: IEEE Trans. Ind. Electron. 61 (2014) 6418. <https://doi.org/10.1109/TIE.2014.2301773>
- 11 B. Xiao and S. Yin: IEEE Trans. Ind. Electron. 68 (2021) 10162. <https://doi.org/10.1109/TIE.2020.3026272>
- 12 Z. Zhou, H. Chen, G. Li, H. Zhong, M. Zhang, and J. Wu: Int. J. Refrig. 125 (2021) 34. <https://doi.org/10.1016/j.ijrefrig.2021.01.009>
- 13 D. Ji, X. Yao, S. Li, Y. Tang, and Y. Tian: Ocean Eng. 232 (2021) 108874. <https://doi.org/10.1016/j.oceaneng.2021.108874>
- 14 Z. Chu, Y. Chen, D. Zhu, and M. Zhang: Ocean Eng. 210 (2020) 107570. <https://doi.org/10.1016/j.oceaneng.2020.107570>
- 15 H. Han, L. Hao, D. Cheng, and H. Xu: PLoS ONE 15 (2020) e0239070. <https://doi.org/10.1371/journal.pone.0239070>
- 16 S. Zhang, Y. Wang, M. Liu, and Z. Bao: IEEE Access 6 (2017) 7675. <https://doi.org/10.1109/ACCESS.2017.2785763>
- 17 J. Lei, C. Liu, and D. Jiang: Renew. Energy 133 (2019) 422. <https://doi.org/10.1016/j.renene.2018.10.031>
- 18 B. Zhang, S. Zhang, and W. Li: Comput. Ind. 106 (2019) 14. <https://doi.org/10.1016/j.compind.2018.12.016>
- 19 G. Betta, C. Liguori, A. Paolillo, and A. Pietrosanto: IEEE Trans. Instrum. Meas. 51 (2002) 1316. <https://doi.org/10.1109/TIM.2002.807987>

- 20 M. A. Saleem, G. Diwakar G, and M. R. S. Satyanarayana: IOSR J. Mech. Civ. Eng. 3 (2012) 08.
- 21 S. Gao, X. Wang, X. Miao, C. Su, and Y. Li: J. Sign. Process. Syst. 91 (2019) 1237. <https://doi.org/10.1007/s11265-019-01463-8>
- 22 X. Gu, Z. Hou, and J. Cai J: Energy and AI 4 (2021) 100056. <https://doi.org/10.1016/j.egyai.2021.100056>
- 23 X. Liu, D. Pei, G. Lodewijks, Z. Zhao, and J. Mei: Adv. Powder Technol. 31 (2020) 2689. <https://doi.org/10.1016/j.apt.2020.04.034>
- 24 X. Deng, Q. Liu, Y. Deng, and S. Mahadevan: Inf. Sci. 340–341 (2016) 250. <https://doi.org/10.1016/j.ins.2016.01.033>
- 25 M. P. Kemp: In AIAA Scitech 2019 Forum 1959. <https://doi.org/10.2514/6.2019-1959>

About the Authors

Myungjun Kim received his M.S. degree in mechanical engineering from Korea Maritime and Ocean University (KMOU), Busan, Korea, in 2022. He is currently working at the Maritime R&D Center, LIG Nex1 Co., Ltd, Korea. His research interests include control system engineering and underwater robots.

Hyunjoon Cho received his M.S. degree in mechanical engineering from Korea Maritime and Ocean University (KMOU), Busan, Korea, in 2020. He is currently a Ph.D. candidate with both KMOU and Marine Robot Center, Korea Institute of Industrial Technology. His research interests include control system engineering, underwater dynamics, underwater robots, and fault detection and diagnosis.

Ki-Beom Choo is currently studying for his master's degree in mechanical engineering and is a full-time researcher at Korea Maritime and Ocean University. His work focuses on unmanned marine vehicles and fault diagnosis, especially unmanned surface vehicles and underwater gliders.

Huang Jiafeng received his B.S. and M.S. degrees from Anhui University of Science & Technology (AUST), China, and Korea Maritime & Ocean University (KMOU), Korea, in 2010 and 2021, respectively. He is pursuing his Ph.D. degree in engineering at KMOU, where he is mainly engaged in the design and control simulation of marine equipment.

Dong-Wook Jung received his master's degree in mechanical engineering and is currently a full-time researcher at Korea Maritime and Ocean University. His work focuses on unmanned marine vehicles, especially unmanned surface vehicles and underwater gliders.

Jung-Hyeun Park is currently studying for his B.Sc. degree in mechanical engineering and is a researcher at Korea Maritime and Ocean University. His research interests include fault detection and diagnosis and unmanned marine vehicles.

Ji-Hyeong Lee obtained his master's degree in mechanical engineering and is currently a researcher at Maritime ICT R&D Center of Korea Institute of Ocean Science and Technology. His work focuses on unmanned marine vehicles, especially unmanned surface vehicles.

Sang-Ki Jeong obtained his Ph.D. degree in mechanical engineering and is currently a senior researcher at Maritime ICT R&D Center of Korea Institute of Ocean Science and Technology. His work focuses on unmanned marine vehicles, especially the control and configuration of hardware systems.

Dae-Hyeong Ji received his M.S. degree in mechanical engineering from Korea Maritime and Ocean University, South Korea, in 2016, and his Ph.D. degree in mechanical engineering from Korea Maritime and Ocean University, South Korea, in 2020. His research interests include navigation and control systems, sensors, and intelligent control and robotics.

Hyeung-Sik Choi is a professor of Korea Maritime and Ocean University, and director of Unmanned Ocean Vehicle Center. His work focuses on unmanned marine vehicles, humanoid robots, adaptive control, and digital controllers for mechanical systems, especially unmanned surface vehicles and underwater gliders.

